Ligament size effect in largely cracked tensile structures

Ligament size effect for largely cracked tensile structures

Alberto Sapora[1], Francesco Ferrian[1], Pietro Cornetti[1], Hossein Talebi[2], Majid R. Ayatollahi[2]

[1]*Department of Structural, Geotechnical and Building Engineering, Politecnico di Torino, Corso Duca degli Abruzzi 24, 10129, Torino, Italy.*

[2]*Fatigue and Fracture Research Laboratory, Center of Excellence in Experimental Solid Mechanics and Dynamics, School of Mechanical Engineering, Iran University of Science and Technology, Tehran, Iran.*

Abstract

The influence of the ligament size on the brittle failure behaviour of largely cracked elements is analysed. To this aim, the following tensile infinite geometries are analysed: (i) a double edge cracked plate; (ii) a cylindrical bar with an external circular crack. The configurations can be considered as complementary to the Griffith crack and the Penny shaped crack, respectively. The failure size effect is investigated through a semi-analytical approach by two different methods: the coupled Finite Fracture Mechanics (FFM) criterion and the Cohesive Crack Model (CCM) implementing a Dugdale's type cohesive law. Theoretical predictions are compared with each other and with experimental data obtained by tensile testing PMMA samples containing two collinear cracks. Strength estimations result accurate.

Keywords: Finite Fracture Mechanics, Cohesive Crack Model, double edge cracked plate, cracked cylindrical bar, ligament size effect, brittle failure.

Nomenclature

$2a$	Ligament depth or diameter	l_{ch}	Irwin's length
a_p	Process zone length	P	Uniaxial remote force
a_{pc}	Critical process zone length	(r, θ, y)	Cylindrical coordinates system
E	Young's modulus	t	Specimen thickness
G	Strain energy	w	Crack Tip Opening Displacement (CTOD)
G_c	Critical strain energy	w_c	Critical CTOD
h	Specimen width	w_σ	CTOD due to external loading
K_I	Stress Intensity Factor (SIF)	w_{σ_c}	CTOD due to cohesive stress
K_{Ic}	Fracture toughness	α	Dimensionless ligament size

$K_{I\sigma}$	SIF due to the external loading	δ_c	Dimensionless critical crack advancement or process zone length
$K_{I\sigma_c}$	SIF due to the cohesive stress	σ_c	Material tensile strength
K_{IN}	SIF due to distributed force N	σ_f	Failure net stress
L	Specimen length	σ_{net}	Net stress
l	Finite crack advancement	σ_y	Stress field
l_c	Critical finite crack advancement	ν	Poisson's ratio

1. Introduction

The strength of common structures can be seriously affected by the presence of cracks. Acting as stress raisers, they give rise to local stress concentrations, thus reducing the load-bearing capacity of the structural element. The influence of cracks on structural integrity has been deeply investigated since the well-known works by Griffith (1921) [1], Orowan (1944) [2], Irwin (1957) [3] and others. Their contributions developed the fundamentals that underlie the modern theory of Linear Elastic Fracture Mechanics (LEFM). Accordingly, the crack propagation can be described by a single parameter, the Stress Intensity Factor (SIF), which depends on the geometry and loading conditions. Fracture takes place when the SIF equals its critical value, also known as fracture toughness of the material.

LEFM approaches have been widely proposed to describe the failure behaviour of structures containing different crack shapes and subjected to different loading conditions, from the static to the fatigue regime, see for instance [4]. For LEFM to work, the crack has to be sufficiently large. What does it mean "sufficiently large" is sometimes difficult to realize a priori, and numerical simulations should be carried out to check the soundness of the approach. Indeed, LEFM fails to deal with very short cracks (commonly detected in real elements), according to which the strength approaches that of the material: the SIF tends to vanish and the approach provides an infinite failure load. This drawback can be overcome by introducing a critical distance at which either the SIF or the stress field are evaluated [5].

On the other hand, there are not so many studies addressing the case of very long cracks (according to which the structure is close to fail). Aim of this paper is thus to investigate the effect of the ligament size on the failure behaviour of largely cracked elements, both theoretically and experimentally. Two structural configurations are taken into account: (i) an infinite tensile plate with two collinear sharp cracks; (ii) a cracked infinite cylindrical bar under uniaxial tension. The geometries are somehow linked with each other, the latter being obtained by the revolution of the former around the loading

axis. Moreover, the configurations can be considered as complementary to the Griffith crack and the Penny shaped crack [6], respectively.

As regards the theoretical framework, the coupled Finite Fracture Mechanics approach and the Cohesive Crack Model (CCM) method are taken into account.

FFM is a fracture criterion [7],[8] resting on the assumption of finite crack advance and based on the fulfilment of two coupled conditions: a stress constraint, considering the stress field in front of the crack tip, and an energy requirement, involving the strain energy release rate. The approach is able to catch the transition from a strength- to a toughness-governed regime as the crack length varies [8]. This peculiarity is observed also by implementing the CCM (e.g. [9]), herein developed considering Dugdale's constitutive law. More in detail, the cohesive stress, acting in the process zone ahead of the crack tip, is constant and equal to the ultimate tensile strength of the material. As highlighted in [10],[11], CCM can be expressed by a system of two equations, a stress conditions and an energy balance. Thus, the process zone which characterizes CCM can be seen as the counterpart of the finite crack increment charactering FFM. Fair to excellent agreement were found between FFM and CCM failure predictions for different cracked structures [6],[12],[13],[14],[15],[16].
Finally, as concerns the experimental part, uniaxial tensile tests are carried out on PMMA cracked samples by varying the structural dimension in order to cover the widest possible range of sizes. FFM and CCM results are compared with experimental ones.

2. Geometries under investigation

In this study, two different structural cracked configurations are analysed.

The first one consists of two collinear sharp cracks in an infinite slab (i.e, a double edge cracked plate) under uniaxial (nominal) net tension $\sigma_{net} = P/2a$. Here $2a$ is the ligament depth and P is the uniaxial remote force along y, (r,y) being the Cartesian frame of reference (Fig. 1a). Considering an isotropic and homogenous material, thanks to the symmetry of the geometry, two symmetric cracks are expected to simultaneously initiate from the crack tips along the r-axis.

The stress field and SIF functions related to this geometry are [17]:

$$\sigma_y(r) = \frac{P}{\pi\sqrt{a^2 - r^2}} \tag{1}$$

and [18]:

$$K_{I\sigma} = \frac{P}{\sqrt{\pi a}} \tag{2}$$

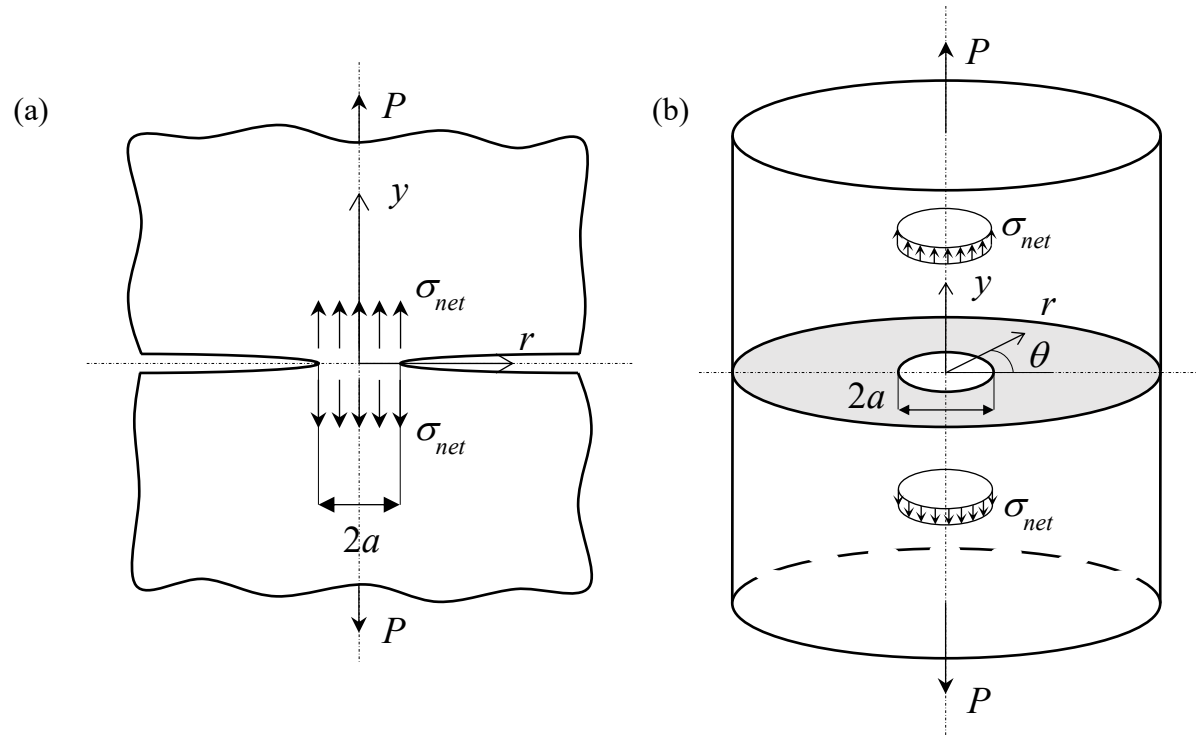

Fig. 1 (a) Double edge cracked plate and (b) cracked cylindrical bar.

The second one is represented by a cracked cylindrical bar subjected to uniaxial net tension $\sigma_{net} = P/\pi a^2$, where $2a$ is the ligament diameter (Fig. 1b). This configuration is obtained through the revolution of a slice of the previous one around the y axis. A cylindrical coordinate system (r, θ, y) is considered, whose origin coincides with the centre of the ligament surface, in the $y = 0$ plane. Thanks again to symmetry, a circular crack is expected to initiate under Mode I opening conditions in the r - θ plane.

For this geometry the stress field can be expressed in the following form [19]:

$$\sigma_y(r) = \frac{P}{2\pi a\sqrt{a^2 - r^2}} \tag{3}$$

whereas the SIF can be expressed as[18]:

$$K_{I\sigma} = \frac{P}{2a\sqrt{\pi a}} \tag{4}$$

Note that relationships (1-4) reveal exact functions [18].

3. Finite Fracture Mechanics

Following the coupled FFM approach, a crack propagates by a finite crack advancement l when a stress requirement and the energy balance are simultaneously satisfied. According to the formulation proposed by Leguillon (2002) [7], the stress condition requires that the normal stress σ_y must exceed the material tensile strength σ_c over a finite distance l. The energy balance ensures that the strain energy G available for a crack increment l is larger than the energy necessary to create the new fracture surface $G_c l$. The condition can be recast considering Irwin's relationship for the SIF $K_{I\sigma} = \sqrt{GE'}$ and fracture toughness $K_{Ic} = \sqrt{(G_c E')}$, E' being the Young's modulus of the material under plain strain conditions. Particularizing FFM formulation to the (positive) geometry containing collinear cracks (Fig. 1a), we have:

$$\begin{cases} \sigma_y\left(r = a - l\right) = \sigma_c \\ \int_{a-l}^{a} K_{I\sigma}^2(a')da' = K_{Ic}^2 l \end{cases} \tag{5}$$

The approach can be also developed considering an average stress condition [8],[20] instead of a punctual one, leading to the present avg-FFM formulation:

$$\begin{cases} \int_{a-l}^{a} \sigma_y(r)dr = \sigma_c l \\ \int_{a-l}^{a} K_{I\sigma}^2(a')da' = K_{Ic}^2 l \end{cases} \tag{6}$$

On the other hand, taking into account the cracked cylindrical bar (Fig. 1b), line integrals must be replaced by surface ones, as the geometry is now three-dimensional. Thus, for this configuration, FFM can be expressed as:

$$\begin{cases} \sigma_y\left(r = a - l\right) = \sigma_c \\ \int_{a-l}^{a} K_{I\sigma}^2(a')2\pi a'da' = K_{Ic}^2 \pi\left[a^2 - \left(a-l\right)^2\right] \end{cases} \tag{7}$$

whereas the following avg-FFM formulation is achieved:

$$\begin{cases} \int_{a-l}^{a} \sigma_y(r)2\pi r dr = \sigma_c \pi\left[a^2 - \left(a-l\right)^2\right] \\ \int_{a-l}^{a} K_{I\sigma}^2(a')2\pi a'da' = K_{Ic}^2 \pi\left[a^2 - \left(a-l\right)^2\right] \end{cases} \tag{8}$$

At failure conditions ($P=P_f$), the unknowns of FFM systems (5) and (7) (or (6) and (8) for the average formulation) are represented by the failure stress σ_f (i.e., the critical value of the net stress σ_{net}) and the critical crack advancement l_c, which results to be a structural parameter, since it depends on both geometry and material properties.

3.1 FFM implementation

Introducing Eqs. (1) and (2) into Eq. (5), FFM can be now implemented for the cracked plate configuration in critical conditions ($P=P_f$):

$$\begin{cases} \dfrac{\sigma_f}{\sigma_c} = \dfrac{\pi}{2}\sqrt{\delta_c\left(2-\delta_c\right)} \\ \dfrac{\sigma_f}{\sigma_c} = \sqrt{\dfrac{\pi}{4\alpha}\dfrac{\delta_c}{\ln\left[1/\left(1-\delta_c\right)\right]}} \end{cases} \tag{9}$$

where $\delta_c = l_c/a$ is the dimensionless critical crack advancement, $l_{ch} = (K_{Ic}/\sigma_c)^2$ is the well known Irwin's length, and $\alpha=a/l_{ch}$ is the dimensionless ligament size. Analogously, considering Eqs. (1), (2) and (6), the avg-FFM can be put in the following form:

$$\begin{cases} \dfrac{\sigma_f}{\sigma_c} = \dfrac{\pi}{2}\delta_c\left[\dfrac{\pi}{2} - \operatorname{atan}\left(\dfrac{1-\delta_c}{\delta_c\sqrt{2/\delta_c-1}}\right)\right]^{-1} \\ \dfrac{\sigma_f}{\sigma_c} = \sqrt{\dfrac{\pi}{4\alpha}\dfrac{\delta_c}{\ln\left[1/\left(1-\delta_c\right)\right]}} \end{cases} \tag{10}$$

On the other hand, the FFM approach can be implemented for the cracked cylindrical bar introducing the stress field (3) and the SIF (4) into either Eq. (7) according to its original formulation

$$\begin{cases} \dfrac{\sigma_f}{\sigma_c} = 2\sqrt{\delta_c\left(2-\delta_c\right)} \\ \dfrac{\sigma_f}{\sigma_c} = \sqrt{\dfrac{2}{\pi\alpha}\left(1-\delta_c\right)\left(2-\delta_c\right)} \end{cases} \tag{11}$$

or Eq. (8) for its average version:

$$\begin{cases} \dfrac{\sigma_f}{\sigma_c} = \sqrt{\delta_c\left(2-\delta_c\right)} \\ \dfrac{\sigma_f}{\sigma_c} = \sqrt{\dfrac{2}{\pi a}l_{ch}\left(1-\delta_c\right)\left(2-\delta_c\right)} \end{cases} \tag{12}$$

Depending on the geometry at hand, FFM estimations are obtained by equalling the right-hand sides of Eq. (9) (cracked plate) or of Eq.(11) (cracked cylindrical bar) to get δ_c through the solution of an implicit equation. This value must be then introduced into one of the two equations in (9) or in (11) in order to obtain the dimensionless failure stress σ_f/σ_c. The avg-FFM systems expressed by Eq. (10) or by Eq. (12) can be solved analogously.

4. Cohesive Crack Model

For the two configurations analysed in this study is possible to achieve semi-analytical solutions even by means of CCM, using a Dugdale-type cohesive law Fig. 2.

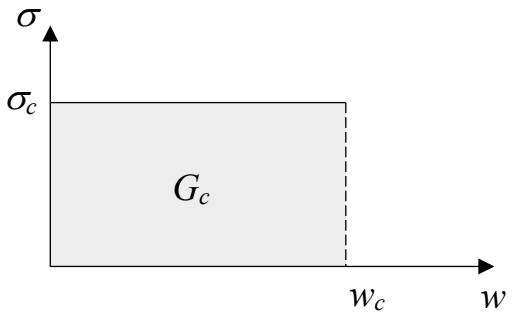

Fig.2 Dugdale's cohesive law.

According to this model, a process zone of length a_p appears in front of the crack tip where the cohesive stress is constant and equal to σ_c (Fig. 3). The length of the process zone a_p increases as the external load increases, till reaching the critical value a_{pc} when σ_{net} equals the failure stress σ_f. To determine the two unknowns, a_{pc} and σ_f, CCM requires the fulfilment of two conditions. The former one is a stress requirement, imposing a vanishing SIF K_I at the fictitious crack tip, $r = a - a_p$, such to eliminate the stress singularity. Considering the superposition principle, K_I can be expressed as a combination of the SIFs due to the external loading $K_{I\sigma}$ and to the cohesive stress $K_{I\sigma_c}$:

$$K_I = K_{I\sigma} - K_{I\sigma_c} = 0 \tag{13}$$

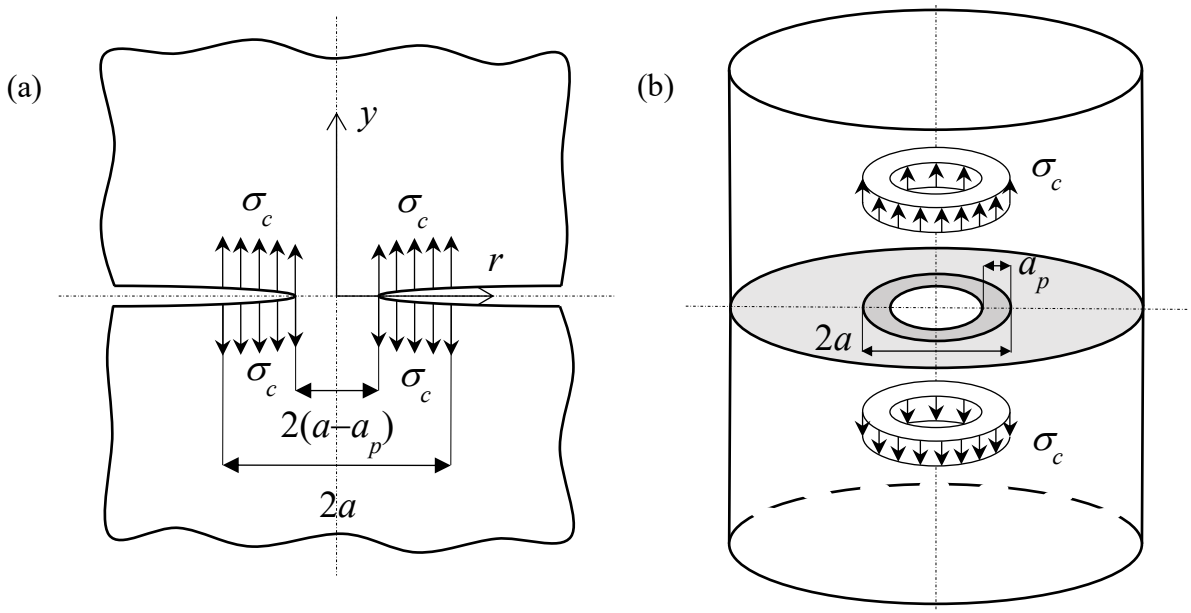

Fig. 3 Cohesive stress σ_c acting on the process zone a_p for the (a) cracked plate and (b) cracked cylindrical bar.

The latter is an energy requirement: crack growth will occur when the crack tip opening displacement (CTOD) reaches the critical value $w_c = G_c/\sigma_c$. Once again, superposition yields:

$$w = w_\sigma - w_{\sigma_c} = w_c \tag{14}$$

where w_σ and w_{σ_c} are the CTODs related to the external loading and the cohesive stress, respectively.

4.1 CCM implementation

In order to implement Eq. (13), the SIFs expressions for $K_{I\sigma}$ are given by Eqs. (2) and (4), whereas those for $K_{I\sigma_c}$ are provided by the SIF handbook [18]:

$$K_{I\sigma_c} = \frac{2\sigma_c}{\sqrt{\pi\left(a-a_p\right)}}\sqrt{a^2-\left(a-a_p\right)^2} \tag{15}$$

$$K_{I\sigma_c} = \pi a^2 \frac{\sigma_c}{\left[\pi\left(a-a_p\right)\right]^{3/2}}\left[\cos^{-1}\frac{a-a_p}{a}+\frac{a-a_p}{a}\sqrt{1-\left(\frac{a-a_p}{a}\right)^2}\right] \tag{16}$$

where Eqs. (15) and (16) refer to the cracked plate and bar, respectively.

On the other hand, in order to manage Eq. (14), the expressions for the CTODs w_σ and w_{σ_c} in the cracked plate are provided by [18]:

$$w_\sigma = \frac{4P}{\pi E'} \cosh^{-1} \frac{a}{a - a_p} \tag{17a}$$

$$w_{\sigma_c} = \frac{8\sigma_c a}{\pi E'} \ln \frac{a}{a - a_p} \tag{17b}$$

whereas those related to the cracked cylindrical bar can be obtained exploiting Paris' equation as:

$$w_\sigma = \frac{2}{E'} \int_0^{a_p} K_{I\sigma} \frac{\partial K_{IN}}{\partial N} \frac{a - t}{a} \mathrm{d}t \tag{18}$$

$$w_{\sigma_c} = \frac{2}{E'} \int_0^{a_p} K_{I\sigma_c} \frac{\partial K_{IN}}{\partial N} \frac{a - t}{a} \mathrm{d}t \tag{19}$$

Here K_{IN} is the SIF related to distributed force N, per unit length, acting at the crack onset point [18] (i.e, a ring):

$$K_{IN} = 2a \frac{N}{\sqrt{\pi \left(a - a_p\right)^3}} \left[\cos^{-1} \frac{a - a_p}{a} + \frac{a - a_p}{\sqrt{a^2 - \left(a - a_p\right)^2}} \right] \tag{20}$$

.

The relationships providing the SIF and CTOD functions through Eqs. (15-20) are exact [18].

Introducing Eqs. (2) and (15) into Eq. (13), the former CCM requirement can be formalized. The latter is achieved considering Eq. (14) and computing the CTODs through Eqs. (17a,b), and exploiting Eqs. (2-4). In formulae:

$$\begin{cases} \dfrac{\sigma_f}{\sigma_c} = \delta_c \sqrt{\dfrac{2}{\delta_c} - 1} \\ \dfrac{\sigma_f}{\sigma_c} = \left[\dfrac{\pi}{4\alpha} + 2 \ln \left(\dfrac{1}{1 - \delta_c} \right) \right] \dfrac{1}{2 \cosh^{-1} \left[1 / \left(1 - \delta_c \right) \right]} \end{cases} \tag{21}$$

where $\delta_c = a_{pc}/a$ is now the dimensionless critical process zone length.

Analogously, considering $K_{I\sigma}$ and $K_{I\sigma_c}$ provided by Eq. (4) and (16), respectively, the CCM for the cracked bar can be put in the following form:

$$\begin{cases} \dfrac{\sigma_f}{\sigma_c} = \dfrac{2}{\pi}\left[\cos^{-1}\left(1-\delta_c\right)+\left(1-\delta_c\right)\sqrt{1-\left(1-\delta_c\right)^2}\right] \\ \dfrac{\sigma_f}{\sigma_c} = \dfrac{1}{2\alpha}+\dfrac{2}{\pi}\displaystyle\int_0^{\delta_c}\left[\cos^{-1}\left(1-t\right)+\left(1-t\right)\sqrt{1-\left(1-t\right)^2}\right]dt \end{cases} \tag{22}$$

where the second equation is obtained computing the CTODs provided by Eqs. (18) and (19). CCM strength estimations through Eqs. (21) and (22) are obtained by a procedure resembling that for the FFM systems (Section 3). The value of δ_c obtained by equalling the right-hand sides of Eq. (21) or (22) must be introduced into one of the two corresponding equations to obtain the dimensionless failure stress σ_f/σ_c.

5. FFM and CCM results

In Sections 4 and 5 we have developed the theoretical framework for the two geometries at hand:

- Cracked plate: FFM, Eq. (9); avg FFM, Eq. (11); CCM, Eq. (21).

- Cracked cylindrical bar: FFM, Eq. (10); avg FFM, Eq. (12); CCM, Eq. (22).

Strength predictions for the first and the second configuration are represented in Figs. 5a and 5b, respectively. Theoretical results show a similar trend for the two geometries. Avg-FFM and CCM both provide a dimensionless failure load $\sigma_f/\sigma_c \to 1$ for vanishing ligaments. Instead, FFM converges to $\pi/2$ (cracked plate) and 2 (cracked cylindrical bar) as $\alpha = a/l_{ch} \to 0$. This represents a drawback of FFM with respect to the two other methods, although not so relevant for the size range of practical interest.

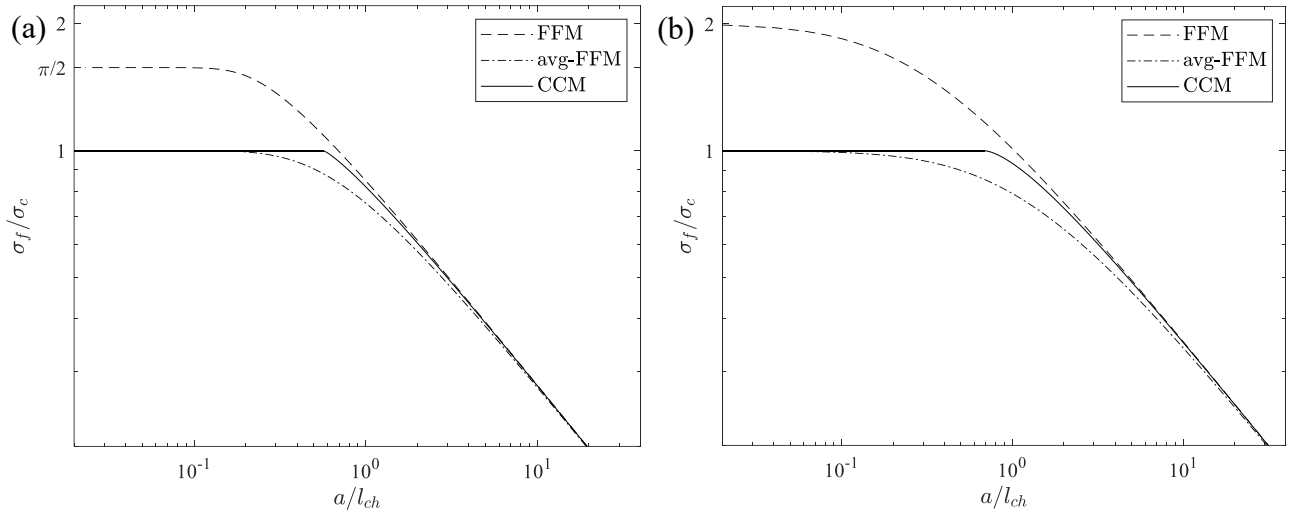

Fig. 5 Strength estimations provided by FFM (dashed line), avg-FFM (dotted-dashed line) and CCM (continuous line) for (a) the cracked plate and (b) the cracked bar.

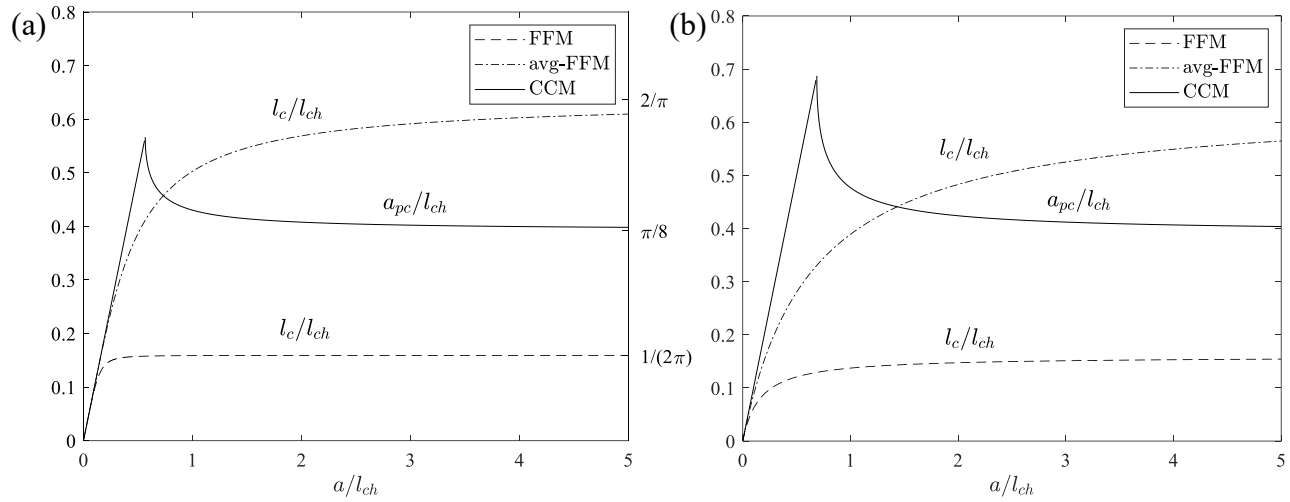

Fig. 6 Critical crack advancement l_c/l_{ch} provided by FFM (dashed line) and avg-FFM (dotted-dashed line), critical process zone length a_{pc}/l_{ch} given by CCM (continuous line) for (a) the cracked plate and (b) the cracked cylindrical bar.

In Figs. 6a and 6b the normalized critical crack advancement l_c/l_{ch} and critical process zone length a_{pc}/l_{ch} are reported as function of the normalized half ligament $\alpha = a/l_{ch}$. Considering FFM, l_c/l_{ch} increases as the ligament increases for both configurations, providing $l_c/l_{ch} \to 1 / (2\pi)$ for $\alpha \to \infty$. A similar trend is detected taking into account avg-FFM, but for the limit $l_c/l_{ch} \to 2/\pi$ for $\alpha \to \infty$. Analogously, also CCM provides a limit value for large ligaments: as α increases, $a_{pc}/l_{ch} \to \pi/8$ (the classical Dugdale's process zone estimate at incipient failure). However, unlike FFM approaches, a_{pc}/l_{ch} increases as a/l_{ch} decreases down to 0.57 for the cracked plate and to 0.69 for the cracked bar. Below these thresholds, a_{pc} solutions by Eqs (21) and (22) become larger than the semi-ligament depth (or radius) a and thus are not acceptable. The actual solution is simply $a_{pc} = a$, i.e. the process

zone covers the whole ligament and $\sigma_f = \sigma_c$.

5.1 Experimental investigation

In order to validate the theoretical framework, uniaxial tensile tests were carried out on double edge cracked PMMA samples (Fig. 7). They were machined from a PMMA sheet by laser cutting. The crack tips were then sharpened by a fresh razor blade, and hence, the effect of the root radius can be considered negligible. In order to catch failure size effects, three different geometries were considered (Table 1, Fig. 8a) and four specimens were tested for each configuration for a total of 12 tested samples. They were characterised by a ratio $a/h = 0.1$ and by a length L at least three times greater than the width h, in order to approach an infinite geometry assumption. Finite element analyses were carried out through ANSYS ® code in order to verify what mentioned above (see also Gupta and Erdogan [21]). Finally, the thickness $t = 5$ mm was set large enough to ensure of the plane strain conditions, satisfying the requirement $t \geq 2.5\ l_{ch}$ [5], l_{ch} being generally comprised between 0.2 mm and 1 mm for PMMA [5],[22].

Experiments were carried out with a constant displacement rate of 0.5 mm/min. The failure loads P_f at which the crack started to propagate are reported in Table 1.

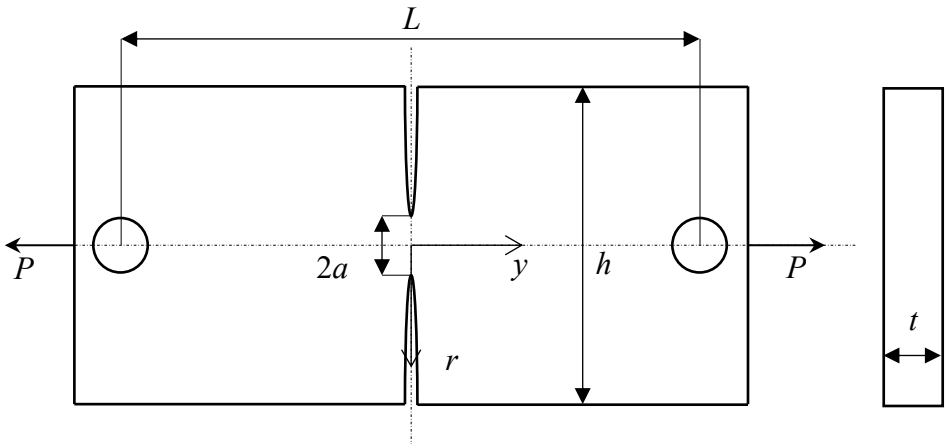

Fig. 7 Geometry of the tensile cracked specimens.

Table 1 Tensile tests on PMMA cracked specimens: Characteristic dimensions and recorded failure loads.

h [mm]	a [mm]	L [mm]	P_f [N]
10	1	90	632.4
			604.8
			661.5
			621.7
20	2	90	841.3
			837.8
			893.7
			-
40	4	150	1245
			1235
			1188
			1161

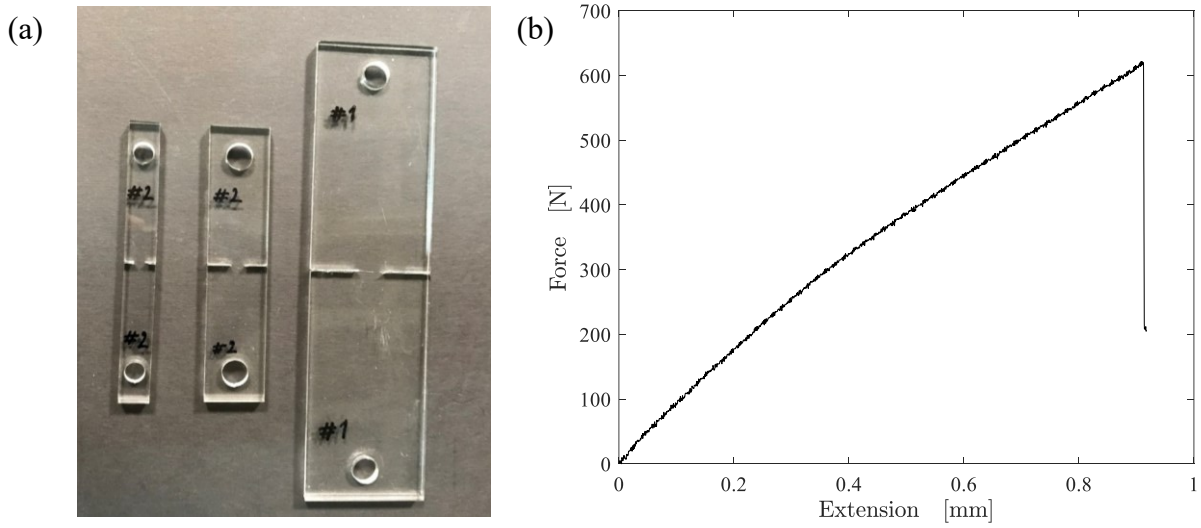

Fig. 8 (a) Three different geometries analysed in the study and (b) force – extension curve obtained for the geometry referring to a = 1 mm.

The failure was of brittle character and plastic deformation was negligible around the crack tip during the tests, as evident from the force – extension curve shown in Fig. 8b.

The mechanical properties for PMMA are reported in Table 2 (note that l_{ch} = 1.02 mm). The ultimate strength σ_c was evaluated experimentally following ASTM D638-14 standard code [23] and testing three dog - bone specimens while employing the Digital Image Correlation (DIC) approach to measure strains (Figs 9a, b).

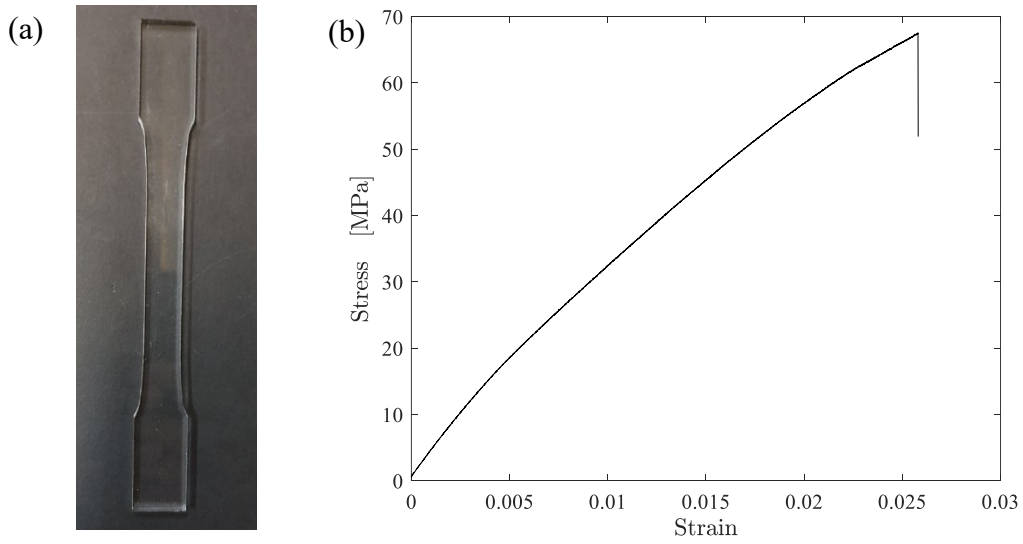

Fig. 9 PMMA: (a) Example of dog – bone specimen and (b) stress – strain curve recorder to determine σ_c.

Analogously to the tensile strength σ_c, also Young's modulus E and Poisson's Ratio v were evaluated experimentally following the procedure described in ASTM D638-14 standard code. Instead, the fracture toughness K_{Ic} was determined based on the results obtained for the largest tested configuration, a = 4 mm, where the crack length is sufficiently large to fall within the LEFM range of validity. Thus, the fracture toughness was computed as $K_I = K_{Ic}$, where K_I is provided by Eq. (2): the value falls in the common range evaluated for PMMA [24],[25] (Table 2).

Table 2 PMMA mechanical properties.

σ_c [MPa]	K_{Ic} [MPa√m]	E [GPa]	v
67.32 ± 0.65	2.15 ± 0.07	2.90 ± 0.11	0.38 ± 0.017

In Fig. 10 the theoretical estimations are plotted against experimental results, showing a fairly good agreement. Indeed, taking into account FFM predictions, the maximum deviation from the average value of the experimental failure stress is equal to 8% for the first configuration (a = 1 mm), 2.5% for

the second (a = 2 mm) and 1% for the third one (a = 4 mm). CCM predictions are nearly the same. Instead, considering avg-FFM, the discrepancy is a little higher: 19%, 8% and 4%, respectively. Note that all the three analysed criteria (FFM, avg-FFM and CCM) provide conservative failure estimations.

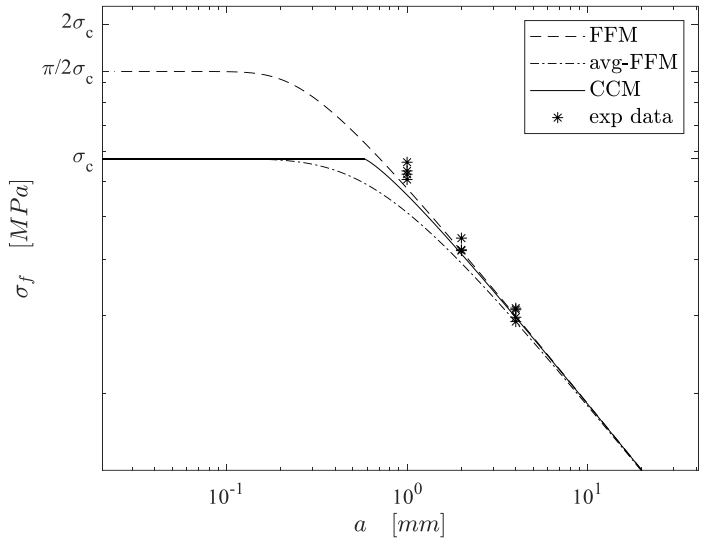

Fig. 10 Tensile tests on PMMA specimens: comparison between experimental results and strength estimations provided by FFM (dashed line), avg-FFM (dotted-dashed line) and CCM (continuous line).

The theoretical deviations from experimental results might depend on the value of σ_c considered in the calculations. Indeed, the failure mechanism of PMMA plain specimens is always influenced by the presence of micro-cracks/defects and crazing phenomena [5],[26]. Thus, the effective tensile strength can be higher than that evaluated experimentally, up to twice [5],[27]. Considering an ultimate strength equal to 80 MPa, for instance, yields a maximum deviation equal to 7% for FFM and to 15% for avg-FFM. Finally, it should be underlined that LEFM results match quite well the above data. Unfortunately, it was not possible to machine and test smaller samples, in order to fully investigate the range where LEFM predictions reveal meaningless (a < 1 mm). Testing materials which are less brittle than PMMA would probably allow to overcome this drawback.

6. Conclusions

1. The failure behaviour of largely cracked structures was investigated by two different approaches: FFM and CCM. Two geometries were analysed: a double edge cracked plate and a circularly cracked cylindrical bar.
2. Both FFM and CCM are based on the fulfilment of a stress requirement and an energy condition, resulting in a crack extension/process zone depending on the ligament size.

3. The analysis was developed semi-analytically for both criteria through the exact functions for the stress field, the SIFs and the CTODs available in the Literature.
4. Whereas avg-FFM and CCM predictions showed a reasonable failure trend, FFM failed to predict the failure stress at small size providing a value higher than the tensile strength.
5. Experimental tests were carried out on double edge cracked tension samples made of PMMA. Despite what underline before, FFM reveals the most accurate criterion for failure stress predictions.

References

[1] Griffith Alan Arnold, VI. The phenomena of rupture and flow in solids, Philos. Trans. R. Soc. London. Ser. A, Contain. Pap. a Math. or Phys. Character. 221 (1921) 163–198. https://doi.org/10.1098/rsta.1921.0006.

[2] E. Orowan, The Fatigue of Glass Under Stress, Nature. 154 (1944) 341–343. https://doi.org/10.1038/154341a0.

[3] G.R. Irwin, Analysis of Stresses and Strains Near the End of a Crack Traversing a Plate, J. Appl. Mech. 24 (1957) 361–364. https://doi.org/10.1115/1.4011547.

[4] K.B. Broberg, Cracks and fracture, Elsevier, Cambridge, 1999.

[5] D. Taylor, The Theory of Critical Distances, Elsevier, London, 2007. https://doi.org/10.1016/B978-0-08-044478-9.X5000-5.

[6] P. Cornetti, A. Sapora, Penny-shaped cracks by Finite Fracture Mechanics, Int. J. Fract. 219 (2019) 153–159. https://doi.org/10.1007/s10704-019-00383-9.

[7] D. Leguillon, Strength or toughness? A criterion for crack onset at a notch, Eur. J. Mech. - A/Solids. 21 (2002) 61–72. https://doi.org/10.1016/S0997-7538(01)01184-6.

[8] P. Cornetti, N. Pugno, A. Carpinteri, D. Taylor, Finite fracture mechanics: A coupled stress and energy failure criterion, Eng. Fract. Mech. 73 (2006) 2021–2033. https://doi.org/10.1016/j.engfracmech.2006.03.010.

[9] A. Needleman, An analysis of decohesion along an imperfect interface, in: Non-Linear Fract., Springer Netherlands, Dordrecht, 1990: pp. 21–40. https://doi.org/10.1007/978-94-017-2444-9_2.

[10] A. Chao Correas, M. Corrado, A. Sapora, P. Cornetti, Size-effect on the apparent tensile

strength of brittle materials with spherical cavities, Theor. Appl. Fract. Mech. 116 (2021) 103120. https://doi.org/10.1016/j.tafmec.2021.103120.

[11] F. Ferrian, P. Cornetti, L. Marsavina, A. Sapora, Finite Fracture Mechanics and Cohesive Crack Model: Size effects through a unified formulation, Frat. Ed Integrità Strutt. 16 (2022) 496–509. https://doi.org/10.3221/IGF-ESIS.61.33.

[12] P. Cornetti, A. Sapora, A. Carpinteri, Short cracks and V-notches: Finite Fracture Mechanics vs. Cohesive Crack Model, Eng. Fract. Mech. 168 (2016) 2–12. https://doi.org/10.1016/j.engfracmech.2015.12.016.

[13] P. Cornetti, M. Muñoz-Reja, A. Sapora, A. Carpinteri, Finite fracture mechanics and cohesive crack model: Weight functions vs. cohesive laws, Int. J. Solids Struct. 156–157 (2019) 126–136. https://doi.org/10.1016/j.ijsolstr.2018.08.003.

[14] P.L. Rosendahl, P. Weißgraeber, N. Stein, W. Becker, Asymmetric crack onset at open-holes under tensile and in-plane bending loading, Int. J. Solids Struct. 113–114 (2017) 10–23. https://doi.org/10.1016/j.ijsolstr.2016.09.011.

[15] A. Doitrand, R. Estevez, D. Leguillon, Comparison between cohesive zone and coupled criterion modeling of crack initiation in rhombus hole specimens under quasi-static compression, Theor. Appl. Fract. Mech. 99 (2019) 51–59. https://doi.org/10.1016/j.tafmec.2018.11.007.

[16] I.G. García, M. Paggi, V. Mantič, Fiber-size effects on the onset of fiber–matrix debonding under transverse tension: A comparison between cohesive zone and finite fracture mechanics models, Eng. Fract. Mech. 115 (2014) 96–110. https://doi.org/10.1016/j.engfracmech.2013.10.014.

[17] F. Erdogan, Stress Distribution in a Nonhomogeneous Elastic Plane With Cracks, J. Appl. Mech. 30 (1963) 232–236. https://doi.org/10.1115/1.3636517.

[18] H. Tada, P.C. Paris, G.R. Irwin, The Stress Analysis of Cracks Handbook, Third Edition, ASME Press, 2000. https://doi.org/10.1115/1.801535.

[19] I.N. Sneddon, Fourier Transforms, McGraw-Hill, New York, 1951.

[20] A. Carpinteri, P. Cornetti, N. Pugno, A. Sapora, D. Taylor, Generalized fracture toughness for specimens with re-entrant corners: Experiments vs. theoretical predictions, Struct. Eng. Mech. 32 (2009) 609–620. https://doi.org/10.12989/sem.2009.32.5.609.

[21] G.D. Gupta, F. Erdogan, The Problem of Edge Cracks in an Infinite Strip, J. Appl. Mech. 41 (1974) 1001–1006. https://doi.org/10.1115/1.3423423.

[22] A. Seweryn, Brittle fracture criterion for structures with sharp notches, Eng. Fract. Mech. 47 (1994) 673–681. https://doi.org/10.1016/0013-7944(94)90158-9.

[23] ASTM D638-14, Standard test method for tensile properties of plastics, in: ASTM Int., West Conshohocken, PA, 2014: pp. 1–15

[24] P. Cornetti, A. Sapora, A. Carpinteri, T-stress effects on crack kinking in Finite Fracture Mechanics, Eng. Fract. Mech. 132 (2014) 169–176. https://doi.org/10.1016/j.engfracmech.2014.10.011.

[25] A. Doitrand, R. Estevez, D. Leguillon, Experimental characterization and numerical modeling of crack initiation in rhombus hole PMMA specimens under compression, Eur. J. Mech. - A/Solids. 76 (2019) 290–299. https://doi.org/10.1016/j.euromechsol.2019.04.013.

[26] J. Hebel, R. Dieringer, W. Becker, Modelling brittle crack formation at geometrical and material discontinuities using a finite fracture mechanics approach, Eng. Fract. Mech. 77 (2010) 3558–3572. https://doi.org/10.1016/j.engfracmech.2010.07.005.

[27] S. Cicero, V. Madrazo, I.A. Carrascal, Analysis of notch effect in PMMA using the Theory of Critical Distances, Eng. Fract. Mech. 86 (2012) 56–72. https://doi.org/10.1016/j.engfracmech.2012.02.015.